

---

# ReLaX-VQA: Residual Fragment and Layer Stack Extraction for Enhancing Video Quality Assessment

---

Xinyi Wang, Angeliki Katsenou, and David Bull

Visual Information Lab, School of Computer Science,  
University of Bristol, Bristol BS1 8UB, UK

{xinyi.wang, angeliki.katsenou, dave.bull}@bristol.ac.uk

## Abstract

With the rapid growth of User-Generated Content (UGC) exchanged between users and sharing platforms, the need for video quality assessment in the wild has emerged. UGC is mostly acquired using consumer devices and undergoes multiple rounds of compression or transcoding before reaching the end user. Therefore, traditional quality metrics that require the original content as a reference cannot be used. In this paper, we propose ReLaX-VQA, a novel No-Reference Video Quality Assessment (NR-VQA) model that aims to address the challenges of evaluating the diversity of video content and the assessment of its quality without reference videos. ReLaX-VQA uses fragments of residual frames and optical flow, along with different expressions of spatial features of the sampled frames, to enhance motion and spatial perception. Furthermore, the model enhances abstraction by employing layer-stacking techniques in deep neural network features (from Residual Networks and Vision Transformers). Extensive testing on four UGC datasets confirms that ReLaX-VQA outperforms existing NR-VQA methods with an average SRCC value of 0.8658 and PLCC value of 0.8872. We will open source the code and trained models to facilitate further research and applications of NR-VQA: <https://github.com/xinyiW915/ReLaX-VQA>.

## 1 Introduction

Video Quality Assessment (VQA) is critical for optimising user experience in video streaming. However, due to the explosion of User-Generated Content (UGC) on video sharing platforms such as YouTube and TikTok [1], VQA has become increasingly challenging. In UGC use cases, videos are typically first encoded on the user’s device (smartphones, consumer cameras, etc) while being captured, and then transcoded by the platform for distribution and storage. As a result of repeated lossy compression, video quality is degraded by the introduction of noticeable artefacts such as blocking, ringing, and blurring [2, 3].

Traditional VQA methods that rely on comparing the distorted video with a reference video, using measures such as Peak Signal-to-Noise Ratio (PSNR) and Structural Similarity Index (SSIM) [4], cannot be reliably used for UGC, as the uploaded video to the sharing platform is not the original. Similarly, learning-based full reference methods, such as Video Multi-Method Assessment Fusion (VMAF)[5], cannot capture the quality of transcoded content because it has been trained on pristine original references and only once-compressed content. Therefore, developing No-Reference Video Quality Assessment (NR-VQA) models for evaluating these types of no-reference video content is imperative.

Over the past few years, Deep Neural Networks (DNNs) have been used to devise advanced NR-VQA models. The robust representation learning capability of DNNs has positioned them as the prime technique for tackling visual tasks[6]. Such models usually employ 2D-CNN, 3D-CNN, and

Transformers[7, 8, 9, 10, 11, 12, 13] and are designed to analyse pixel variations due to compression and correlations to subjective quality scores. Existing models are primarily frame-based and struggle to capture temporal impairments effectively. Furthermore, the resizing of frames causes further degradation, which has driven the development of VQA models focused on fragments[14, 13]. Despite their efficiency, DNN VQA models are resource-thirsty (high computational complexity) and data-hungry (requiring large volumes of data for training) [15]. Thus, the unavailability of large-scale datasets with subjective scores to train these networks from scratch limits their performance. Therefore, many existing VQA models rely on networks that are pre-trained on large image classification datasets to extract frame-based features[8, 9, 16, 17]. Although results look promising, this practice can result in a distributional shift between the original training task and the actual VQA application task. Moreover, despite the importance of frame-level spatial information, temporal information (motion or inter-frame variations) needs to be accounted to evaluate the video quality accurately.

In response to these challenges, we introduce ReLaX-VQA, a feature extractor that utilises two main techniques: spatio-temporal fragmentation (residual and optical flow) and layer stacking. In consideration of the residual between successive frames, inspiration is drawn from the structure of current block-based video encoders (e.g., H.264 [18] or H.265 [19]), where the frame encoding follows a hierarchical structure within a group of frames, with more bits allocated for the encoding of keyframes (I frames) and fewer for the successive predicted frames (P frames). Thus, the quality of the decoded frames varies per frame and is typically higher for I frames. Therefore, when subtracting two successive frames, key and a predicted, the residual is an expression of both the temporal information in moving regions as well as spatial artefacts around areas with compression artefacts. This residual information can be exploited to correlate it with the perceptual variations in the Human Visual System (HVS). As this residual is sparse, we propose the extraction of residual fragments. The selection of the fragments is based on the ranking of residuals (absolute difference) on the basis that human attention is drawn to areas with visible distortions. Fragmenting is also applied to temporal information, particularly to optical flow, which can reveal regions in the frame undergoing the most dynamic changes. This method can effectively utilise the motion information to enhance the perception of the model. We also selected patches from locations of prominent dynamic changes in the sample frame. The second technique relies on a layer-stacking DNN feature extraction. Unlike pooling, this enhances the representation of deep features and increases their relevance to human perception. Through visualisation and perceptual correlation, we identified that different network layers capture information at different levels, from edges to abstract features. This hierarchical feature extraction mechanism allows our model to mimic human visual processing more closely, thereby achieving more precise visual perception in complex scenarios.

Finally, to further improve the prediction performance of the extracted features, we constructed a simple and efficient Multi-Layer Perceptron (MLP) regression head for training and testing. By combining the characteristics of the Residual Network (ResNet) [20] focusing on local information, and the advantages of the Vision Transformer (ViT) [21] which concentrates on global features, our method improves the prediction accuracy. The contributions of this work are summarized below:

1. We propose ReLaX-VQA, a novel NR-VQA model that focuses on extracting fragmented information from frame differencing and optical flow fields between consecutive frames to enhance spatio-temporal perception.
2. We boost the feature abstraction capabilities by layer-stacked feature extraction. The layer stacking technique has proven effective in information fusion.
3. We provide an improved design of MLP regression that fuses local and global features for higher accuracy.

The proposed model, ReLaX-VQA, has undergone extensive testing on several public large-scale datasets. The results, assessed by linear and rank correlation coefficients with mean opinion scores, Spearman (SRCC), Kendal (KRCC), and Pearson (PLCC), as well as Root Mean Square Error (RMSE), indicate higher accuracy, outperforming existing NR-VQA methods. Our model is straightforward to implement and computationally efficient. We will make the source code and pre-trained models available for public research and use.

Table 1: Summary of VQA benchmark datasets

Dataset	Resolution	Duration	Distortion	Subjective framework	Size
CVD2014[22]	480p, 720p	10-25s	In-capture	In-lab	234
KoNViD-1k[23]	540p	8s	In-the-wild	Crowdsourced	1,200
LIVE-VQC[24]	240p-1080p	10s	In-the-wild	Crowdsourced	585
YouTube-UGC[3]	360p-4k	20s	In-the-wild	Crowdsourced	1,149*
LSVQ[10]	99p-4k	5-12s	In-the-wild	Crowdsourced	38,793**

## 2 Related work

### 2.1 UGC video datasets

To develop more realistic and accurate VQA models for UGC content, numerous datasets have been created. Table 1 reports commonly used subjective video quality datasets used in recent studies. CVD2014 [22] and LIVE-VQC [24] are datasets that simulate distorted videos from online video streaming through compression and transmission distortion, and artificial distortions (e.g., Gaussian blurring)[25]. These datasets are small and contain only a limited number of unique source videos with restricted content diversity and distortion complexity. On the other hand, video quality databases collected “in the wild” specifically for UGC are constantly being updated. These collections include a large number of real distorted videos produced by amateurs and more accurately reflect the complexities of UGC videos. Examples are the LIVE-Qualcomm[26], KoNViD-1k[23], YouTube-UGC[3], and LIVE-VQC[24]. Although these datasets are larger and contain more content variation, they are still insufficient to train deep learning models. The recent release of two large-scale VQA datasets: FlickrVid-150k[27] (not publicly available) and LSVQ[10] tried to address the lack of training data for deep learning-based VQA models. Notably, the publicly available LSVQ dataset, which contains 39,076 videos, demonstrates advantages in handling large-scale video data.

### 2.2 NR VQA models

Numerous classic NR-VQA models have been developed based on traditional Natural Scene Statistics (NSS), such as NIQE[28], PIQE[29], and BRISQUE[30]. Inspired by frequency domain characteristics, V-BLIINDS[31] and V-CORNIA[32] used Discrete Cosine Transform (DCT) statistics and learned codebooks to mark image integrity and block features respectively. These methods perform better for specific types of distortions (e.g., blurriness) and have been designed to capture a specific range of video quality. Other models employ a large number of handcrafted features and feature selection strategies to evaluate video quality. Successful examples are TLVQM[33] and VIDEVAL[34]. TLVQM combines high spatial complexity and low temporal complexity features, while VIDEVAL integrates a wide range of handcrafted features to simulate real distortions. These models train shallow regression models with statistical features and perform well on standard video (not UGC) content, but are limited in generalising over UGC content.

More recently, VQA research has shifted towards DNNs, such as CNNs and Transformers for constructing feature extractors. Notably, RAPIQUE [9], combines NSS with semantic-aware CNN features extracted from downsampled frames, resulting in reduced computational runtime. Another high-performing model is VSFA[8] and its enhanced version, MDTVSFA[35] (using a hybrid dataset training strategy), that extracts frame features using the pre-trained image classification model ResNet-50[20] and apply gated recursive units to process temporal features. The latest developments in NR-VQA focus on addressing multi-resolution and complex spatio-temporal distortions in UGC. Using patches and fragments as in [10, 14, 13] and/or novel data sampling mechanisms as in [36, 37] helps preserve the global and local details of high-resolution videos, capturing complex spatio-temporal features and improving processing efficiency. Other NR-VQA models perform end-to-end feature training or multi-scale feature fusion, utilising attention mechanisms and simulating HVS features to enhance performance[14, 38, 39, 11]. An important aspect of VQAs is the ranking ability and therefore Chen et al [40] focus on improving the ranking performance of their model by using VMAF-based quality ranking information but train their model on standard video datasets with access to uncompressed content. Li et al.[41] address domain bias by transferring knowledge from image

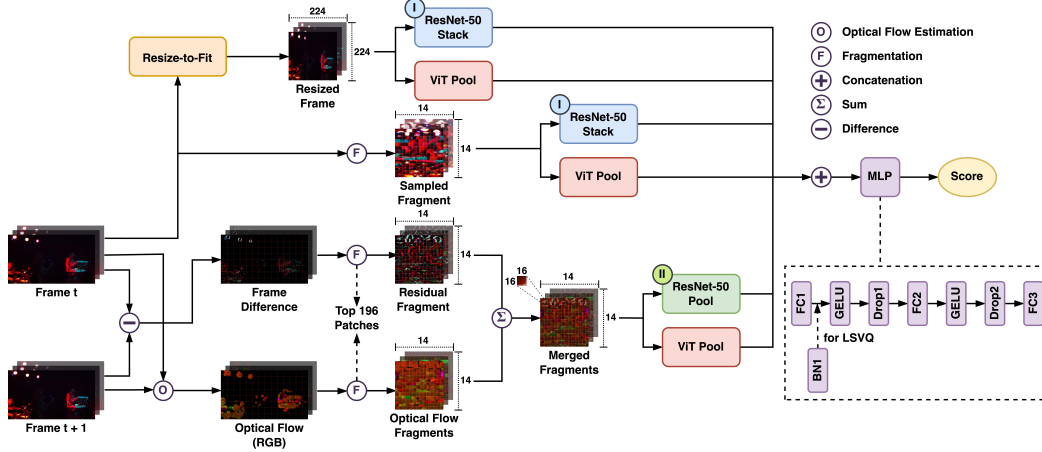


Figure 1: Overview of the proposed ReLaX-VQA framework that demonstrates the different processing of the input frames for the feature extraction and regression to infer the quality score. The architectures of ResNet-50 Stack (I) and ResNet-50 Pool (II) are provided in Fig. 2 in the Appendix.

quality and motion recognition databases to improve benchmarks. UVQ[42] further augments the video quality metrics by incorporating semantic information.

### 3 Proposed method

An overview of the proposed ReLaX-VQA model framework is provided in Fig. 1 and consists, from bottom to top, of the spatio-temporal fragment sampling module (Section 3.1), DNN Layer stack module (Section 3.2), and quality regression module (Section 3.3). Firstly, we extracted features from successive sampled video frames using the spatio-temporal fragment sampling module from frame differencing (residuals) and optical flow. Then, we stacked the extracted features using different layers of the deep neural network, fusing these multi-layered features to capture the quality-aware features. Finally, a simple MLP quality regression module maps the quality-aware features to video quality scores. Furthermore, we introduced a hybrid Mean Absolute Error (MAE) and Rank loss function to optimise the quality prediction model. Through this approach, ReLaX-VQA can effectively utilise the residual information after dynamic changes between video frames. The local and global information that affects the video quality is captured through feature layer stacking, enhancing the model’s abstraction capability and its consistency with human perception.

#### 3.1 Spatio-temporal fragment sampling module

Frequently in VQA, researchers resize or crop frames prior to feature extraction. Resizing often introduces quality degradation as it filters or changes local textures, which are often critical in the perception of video quality, while cropping affects the alignment of global and local quality. Particularly at high spatial resolutions, these processing methods might result in a significant loss of detail. Moreover, the viewer does not only notice the overall quality but also temporal artefacts, e.g., sudden object transitions/deformations due to motion estimation errors, and/or any other spatial artefacts, e.g., blocking artefacts, colour bleeding. By extracting the key fragments with the highest dynamic changes from frame to frame, we can effectively capture both local and global information affecting video quality. Most UGC videos are short, usually containing only one shot, and redundancy in spatio-temporal information especially at high frame rates. Therefore, we propose an innovative Residual Fragment (RFs) sampling method to capture the effect of motion and spatial variations on video quality.

We sampled the video at a rate of two frames every half second to obtain successive and temporally correlated frame pairs  $F_t$  and  $F_{t+1}$ . We first computed the frame difference  $\Delta F_t(x, y)$  by calculating the absolute difference of each pixel in between the extracted frame pairs to capture the inter-frame content variations, as follows:

$$\Delta F_t(x, y) = |F_{t+1}(x, y) - F_t(x, y)|, \quad (1)$$

---

**Algorithm 1** Spatio-temporal Residual Fragment Extraction
 

---

1: **Input:** Frame difference or optical flow  $F$ , Patch size  $p$ , Target image size  $n$ , Top- $K$  patches  
 2: **Output:** Patches matrix  $P$ , Patch positions  $P_{\text{positions}}$ , Residual fragments  $RF$ ,  
 3: Initialise matrix  $P \leftarrow 0$   
 4: **for**  $i = 0$  to  $\text{height} - p$  **do**  
 5:     **for**  $j = 0$  to  $\text{width} - p$  **do**  
 6:         Extract patch:  $\text{patch} \leftarrow F[i : i + p, j : j + p]$   
 7:         Calculate sum:  $P_{\Delta F_t}(i, j) \leftarrow (4)$  ▷ For frame difference  
 8:          $P_{f_t}(i, j) \leftarrow (4)$  ▷ For optical flow  
 9:     **end for**  
 10: **end for**  
 11: Find top- $K$  patches:  $\text{top\_idx} \leftarrow \text{sort}(\text{argsort}(P, K))$   
 12: Initialise  $RF \leftarrow 0$  and  $P_{\text{positions}} \leftarrow []$   
 13: **for** each index  $(y, x)$  in  $\text{top\_idx}$  **do**  
 14:     Extract patch:  $\text{patch} \leftarrow P[y \cdot p : (y + 1) \cdot p, x \cdot p : (x + 1) \cdot p]$   
 15:     Determine new location in the target image  $I_{\text{patches}}$  (size:  $n \times n$ ):

$$\text{row\_idx} \leftarrow \left\lfloor \frac{\text{idx}}{\lfloor \frac{n}{p} \rfloor} \right\rfloor, \quad \text{col\_idx} \leftarrow \text{idx} \bmod \left\lfloor \frac{n}{p} \right\rfloor$$

16:     Insert patch into  $RF$  and update  $P_{\text{positions}} \leftarrow P_{\text{positions}} \cup \{(y, x)\}$   
 17: **end for**  
 18: **return**  $P, RF, P_{\text{positions}}$

---

where  $(x, y)$  represents the pixel position, and  $|\cdot|$  denotes the absolute value. In most scenes, there is less variation in the static background between successive frames, whereas moving objects or shifts in the background caused by camera movement can produce higher pixel differences.

Concurrently, to better capture motion information, we applied Farneback dense optical flow estimation [43] to quantify pixel motion across video frames based on temporal continuity and spatial luminance consistency. Optical flow  $f_t(x, y)$  is computed by comparing the pixel positions between consecutive frames  $F_t$  and  $F_{t+1}$  to estimate the direction and velocity of movement of each reference pixel  $(x, y)$ , by solving the following equation:

$$F_t(x, y) \approx F_{t+1}(x + \delta x, y + \delta y), \quad (2)$$

where  $\delta x$  and  $\delta y$  are the horizontal and vertical components, representing the predicted movement distance of pixel  $(x, y)$ . For easier visualisation of the motion in the colour space, we converted the magnitude and angle of the optical flow vectors into colour information and transformed the colour space from HSV to RGB:

$$\text{RGB} = \text{HSVtoRGB} \left( \left( \left[ \frac{\arctan 2(v, u)}{\pi} \times 180, 2^b - 1, \min \left( \frac{\sqrt{u^2 + v^2}}{\max(|\mathbf{F}|)}, 1 \right) \times (2^b - 1) \right] \right) \right), \quad (3)$$

where  $\mathbf{F}$  represents the entire optical flow field, with the optical flow vector at each point consisting of horizontal components  $u$  and vertical components  $v$ , and  $b$  is the bit-depth.

After computing  $\Delta F_t$  and  $f_t(x, y)$ , we extracted regions with high residual information, termed ‘‘top patches’’. We uniformly segmented the frame difference and optical flow into fixed-size pixel patches ( $p \times p$ ). For each patch, we computed the following sums:

$$S_{\Delta F_t}(i, j) = \sum_{x=i}^{i+p} \sum_{y=j}^{j+p} \Delta F_t(x, y) \quad \text{and} \quad S_{f_t}(i, j) = \sum_{x=i}^{i+p} \sum_{y=j}^{j+p} \|f_t(x, y)\|, \quad (4)$$

where  $S_{\Delta F_t}(i, j)$  and  $S_{f_t}(i, j)$  are the sum of frame differences and the sum of optical flow magnitudes  $\|f_t(x, y)\|$  in the patch  $(i, j)$ , respectively.

The selected top patches from the frame differencing and optical flow are mapped into a merged fragment, MF, which retains the most salient regions of variation in the time series while discarding

the static or low residual information:

$$MF(x, y) = \alpha \cdot RF_{\Delta F}(x, y) + (1 - \alpha) \cdot RF_f(x, y), \quad (5)$$

where  $MF(x, y)$  is the merged fragment and  $\alpha = 0.5$  is a weighting parameter for the two fragments,  $RF_{\Delta F}$  and  $RF_f$ . The target RFs are sized at  $224 \times 224$  pixels to align with the model input requirements. We set the size of the top patches to  $p \times p$  (where  $p = 16$ ) pixels, arranging them in a  $14 \times 14$  grid to achieve the target dimensions. Consequently, a total of 196 important patches need to be selected. This process is detailed in Algorithm 1(line 11). We also extracted patches from the same positions as the top frame difference patches to construct sampled spatial fragments, based on the principle of spatial position invariance. This sampling criterion is based on the hypothesis that patches with higher residual information (indicating increased movement or variation) are critical for understanding changes in video content and are more likely to convey noticeable compression artefacts. We also provided two example videos to visualise the merged fragments in Fig. 3 in the Appendix.

### 3.2 DNN layer stack module

We observed that the lower (first) layers of CNN networks process basic image elements such as edges, colours, and textures, while deeper layers handle advanced more abstract information. Recent studies[44, 45] indicated that saliency features may be inherent in representations of different DNN layers (not in just pooled flattened features), allowing us to simulate human attention to regions of interest. Therefore in this work we used layer stacking and global pooling techniques to enhance DNN features and improve the perceptual accuracy of the prediction model. Besides this, through the integration of ViT features [21], which focus on global information, with ResNet-50[20] features, which focus on local details, we can further improve the model’s ability to process complex visual information. To support this, we conducted an ablation study to evaluate the impact of using different features alone, further validating the proposed method (see Section 4, Table 4).

For each layer  $n$  of ResNet-50, the feature map  $m^{(n)}(x)$  possesses dimensions  $C_n \times H_n \times W_n$ , where  $C_n$  represents the number of channels,  $H_n$  represents the height, and  $W_n$  represents the width. The channel mean is computed for each channel  $c$  in the  $n$  layer. The feature vectors  $v^{(C_n)}$  from each layer are concatenated to form a layer-stacked feature comprising all the layer features:

$$v^{(n)}_c = \frac{1}{H_n \times W_n} \sum_h h = 1^{H_n} \sum_{w=1}^{W_n} m^{(n)}(x_{c,h,w}) \quad (6)$$

$$V_{\text{CNN}}^{\text{stack}} = v^{(1)} \oplus v^{(2)} \oplus \dots \oplus v^{(C_i)} \quad (7)$$

Along with layer stacking, we also applied global pooling components to the network, computing average pooling, maximum pooling and standard pooling:

$$\mu = \text{mean}(m^{(n)}(x)), \quad \zeta = \text{max}(m^{(n)}(x)), \quad \sigma = \text{std}(m^{(n)}(x)) \quad (8)$$

Here,  $m(x)$  is defined differently in different networks. In ResNet-50,  $m(x)$  refers to the feature (avg\_pool) following the average pooling layer of the network. Consequently, the enhanced features are shaped by computing global statistics and concatenating them with the avg\_pool feature vectors. In contrast, in ViT,  $f(x)$  refers to the patch embeddings (excluding CLS tokens) output by the encoder, with dimensions  $N \times D$ , where  $N$  denotes the number of patches and  $D$  the dimension of each patch. We performed global pooling directly on the patch embeddings:

$$V_{\text{CNN}}^{\text{pool}} = V_{\text{avg\_pool}} \oplus \mu_{\text{avg\_pool}} \oplus \zeta_{\text{avg\_pool}} \oplus \sigma_{\text{avg\_pool}} \quad (9)$$

$$V_{\text{ViT}}^{\text{pool}} = \mu_{\text{patch\_embedding}} \oplus \zeta_{\text{patch\_embedding}} \oplus \sigma_{\text{patch\_embedding}} \quad (10)$$

Next, we aggregated the enhanced feature vectors from ResNet-50 and ViT to acquire DNN features for the sampled video frames. After processing all the sampled frames, we derived a feature representation of the video sequence by averaging the features of each frame  $V_{\text{video}} = \frac{1}{N} \sum_{i=1}^N (V_{\text{CNN}} \oplus V_{\text{ViT}})$ .

### 3.3 Quality regression module

We designed a simple and efficient MLP [46] regression head to predict video quality scores. The model consists of three fully connected layers, with hidden layers of dimensions 256 and 128, and the last layer outputs the predicted scores. We applied the GELU activation function and a dropout rate of 0.1 after the first two layers, with the final layer directly outputting the results. Throughout the training process, we utilized the SGD optimizer and applied Cosine Annealing learning rate decay[47]. Additionally, we introduced the Stochastic Weight Averaging (SWA)[48] technique to enhance the model’s generalization performance. To prevent overfitting, we adopted an early stopping strategy with a patience of 5 epochs. Moreover, we incorporated batch normalization for handling the large dataset LSVQ[10].

### 3.4 Loss function

We used a composite loss function inspired by [49], where the MAE loss and Rank Loss are weighed by specific weights to achieve optimal learning. Specifically, we introduced two weighting parameters,  $l1_w$  and  $rank_w$ , to adjust the weights of the two losses in the total loss function. MAE loss is used to calculate the average absolute difference between predicted scores and ground truth:

$$L_{MAE} = \frac{1}{n} \sum_{i=1}^n |y_{pred,i} - y_{true,i}|, \quad (11)$$

where  $y_i \in \mathbb{R}$  represents a quality score.

Rank loss encourages the model to maintain the correct ranking by comparing the differences between paired predicted and true values. Since scores on the diagonal compare to themselves, here we excluded the effect of rank on the diagonal. The rank loss  $L_{Rank}$  can be expressed as:

$$L_{Rank} = \frac{1}{n \cdot (n - 1)} \sum_{i=1}^n \sum_{j=1}^n \max(0, \delta_{ij} - e(y_{true,i}, y_{true,j}) \cdot d_{ij}), \quad (12)$$

where  $\delta_{ij} = |y_{true,i} - y_{true,j}|$  represents the absolute difference in true scores, and  $d_{ij} = y_{pred,i} - y_{pred,j}$  represents the difference in predicted scores. The function  $e(y_{true,i}, y_{true,j})$  is defined as follows:

$$e(y_{true,i}, y_{true,j}) = \begin{cases} 1 & , \text{ if } y_{true,i} \geq y_{true,j} \\ -1 & , \text{ otherwise.} \end{cases} \quad (13)$$

Finally, the total loss  $L_{Total}$  helps the model to capture more information about different distortions or different details, thus speeding up convergence, calculated as:

$$L_{Total} = L_{MAE} \times l1_w + L_{Rank} \times rank_w. \quad (14)$$

## 4 Experiments

### 4.1 Experimental setup

**UGC Datasets** Our model’s performance has been evaluated on current state-of-the-art NR-VQA datasets including CVD-2014[22], KoNViD-1k[23], LIVE-VQC[24], and YouTube-UGC[3]. Additionally, we have conducted feature extraction and training on the large-scale LSVQ[10] dataset and successfully migrated to smaller VQA datasets by Fine-Tuning (FT) the pre-trained model, thereby achieving better performance. We excluded 46 greyscale videos from the YouTube-UGC\* dataset, leaving 1,103 videos, and 283 greyscale videos from the LSVQ\*\* dataset, leaving 38,510 videos.

**Evaluation method** We employed evaluation metrics including SRCC, KRCC, PLCC, and RMSE to assess the performance of our NR-VQA model. These metrics evaluate the monotonicity, linearity, and accuracy of the predictions. In this case, PLCC and RMSE are calculated after a nonlinear four-parameter logistic regression[50]. All results will be reported on our project GitHub page, while in Table 2 we only report SRCC and PLCC values.

Table 2: Performance comparison of the evaluated NR-VQA models on the four NR-VQA datasets. The red and blue entries indicate the best and second-best performance on each database for each performance metric, respectively.

Datasets Models/Metrics	CVD2014[22]		KoNViD-1k[23]		LIVE-VQC[24]		YouTube-UGC[3]		Overall	
	SRCC	PLCC	SRCC	PLCC	SRCC	PLCC	SRCC	PLCC	SRCC	PLCC
BRISQUE[30]	0.5553	0.5527	0.6781	0.6746	0.6096	0.6652	0.3517	0.3768	0.5487	0.5673
V-BLIINDS[31]	0.7306	0.7853	0.7258	0.7155	0.6925	0.6872	0.4783	0.4967	0.6568	0.6712
TLVQM[33]	0.5399	0.5785	0.7616	0.7463	<b>0.8133</b>	0.7912	0.6802	0.6876	0.6988	0.7009
VIDEVAL[34]	0.7663	0.8062	0.8073	0.7923	0.7725	0.7752	0.7814	0.7929	0.7819	0.7916
RAPIQUE[9]	0.8530	0.8766	0.8219	0.8191	0.7328	0.7520	0.7994	0.8300	0.8018	0.8194
VSFA†[8]	<b>0.8825</b>	0.8784	0.8067	0.8182	0.5898	0.5894	0.7857†	0.7808†	0.7662	0.7667
<b>ReLaX-VQA (ours)</b>	0.8643	<b>0.8895</b>	<b>0.8535</b>	<b>0.8473</b>	0.7655	0.8079	0.8014	0.8204	<b>0.8212</b>	<b>0.8413</b>
<b>ReLaX-VQA (w/o FT)</b>	0.7845	0.8336	0.8312	0.8427	0.7664	<b>0.8242</b>	<b>0.8104</b>	<b>0.8354</b>	0.7981	0.8340
<b>ReLaX-VQA (w/ FT)</b>	<b>0.8974</b>	<b>0.9294</b>	<b>0.8720</b>	<b>0.8668</b>	<b>0.8468</b>	<b>0.8876</b>	<b>0.8469</b>	<b>0.8652</b>	<b>0.8658</b>	<b>0.8872</b>

**Implementation details** We used ResNet-50[20] pre-trained on ImageNet[51] and ViT-B/16[52] pre-trained models to extract video features. The dataset was split into training, validation, and test sets in a 64%-16%-20% ratio, respectively. For the LSVQ dataset, we applied 10-fold cross-validation, allocating 9 folds for training and 1 fold for validation, to improve the generalization of our MLP model. The training was conducted over 21 iterations, with 20 epochs for the LSVQ dataset and 120 epochs for other smaller datasets. We used a batch size of 256. Specifically, for the LSVQ dataset, SGD was employed with a learning rate of 0.1 and a weight decay of 0.005, while for other datasets, the learning rate was 0.01 with a weight decay of 0.0005. SWA was implemented in the later stages of training with a learning rate of 0.05. Our loss function utilized weight parameters  $l_w = 0.6$  and  $rank_w = 1.0$ . We tested model selection with two criteria: *byrmse*, which selects the best model with the smallest RMSE in the validation set, and *bykrcc*, which selects the best model with the highest KRCC. We evaluated the performance by reporting the median and standard deviation of SRCC and PLCC across 21 iterations. All experiments utilized a workstation with an NVIDIA GeForce RTX 3090 GPU, a 6-core Intel(R) Xeon(R) W-1250 CPU, and 64.0 GB RAM. The proposed model was implemented in PyTorch[53] on Python 3.8.

## 4.2 Performance comparison

We used the following datasets to train and evaluate our proposed model, CVD2014, KoNViD-1k, LIVE-VQC, YouTube-UGC and the largest dataset available, LSVQ. Based on the different strategies for training and testing we created three versions of our proposed method, ReLaX-VQA:

- i ReLaX-VQA: this version was separately trained and tested on each dataset;
- ii ReLaX-VQA (w/o FT): this version was trained on LSVQ dataset and the frozen model was used for testing on the other datasets;
- iii ReLaX-VQA (w/ FT): this version was trained on LSVQ dataset and the frozen model was fine-tuned on the other datasets to fit the new data features better.

For ReLaX-VQA (w/o FT) and ReLaX-VQA (w/ FT) that were trained on LSVQ, we used the official subset  $LSVQ_{train}$  for training and the  $LSVQ_{test}$ , another subset for testing to obtain frozen trained models. Furthermore, we selected the best-trained model based on *byrmse* selection criteria and the results are reported in Table 2. We compare current state-of-the-art models using the correlation metrics SRCC and PLCC, including classical models and deep learning-based NR-VQA models. A first observation is that ReLaX-VQA (w/ FT) delivers the best performance across all datasets, followed by ReLaX-VQA. All ReLaX-VQA versions significantly outperform traditional NSS-based methods, such as BRISQUE. In comparison with the deep learning-based model VSFA, ReLaX-VQA (w/ FT) achieved  $\Delta SRCC = 0.257$  and  $\Delta PLCC = 0.2982$  on LIVE-VQC. ReLaX-VQA (w/o FT) achieves high scores of  $SRCC = 0.8312$  and  $PLCC = 0.8427$  on KoNViD-1k, not inferior to the best ones that are fine-tuned on the target dataset († We need to note that for VSFA evaluation, we excluded the 110 2160p videos from the YouTube-UGC dataset because our GPU could not support them.). Most VQA methods achieve better performance on single-resolution datasets (i.e., KoNViD-1k), but this deteriorates on multi-resolution datasets (i.e., YouTube-UGC, LIVE-VQC). On the other hand, ReLaX-VQA maintains its high performance on datasets covering multiple resolutions. This



Table 3: Ablation study on *spatio-temporal fragment sampling*.

Datasets	KoNViD-1k	
	SRCC	PLCC
frame difference ( <i>ResNet-50</i> )	0.6526	0.6525
optical flow ( <i>ResNet-50</i> )	0.5793	0.5848
frame difference ( <i>ViT</i> )	0.6384	0.6454
optical flow ( <i>ViT</i> )	0.5692	0.5844
$RF_{\text{frame difference}}$ ( <i>ResNet-50</i> )	0.7082	0.7073
$RF_{\text{optical flow}}$ ( <i>ResNet-50</i> )	0.4844	0.4958
$RF_{\text{frame difference}}$ ( <i>ViT</i> )	0.7145	0.7226
$RF_{\text{optical flow}}$ ( <i>ViT</i> )	0.5032	0.5335
<b>MF (<i>ResNet-50</i>)</b>	0.6792	0.6788
<b>MF (<i>ViT</i>)</b>	0.7062	0.7057
<b>MF (<i>ResNet-50+ViT</i>)</b>	0.7324	0.7291

Table 4: Ablation study on *DNN layer stack*.

Datasets	KoNViD-1k	
	SRCC	PLCC
VGG-16 ( <i>pool</i> )	0.6665	0.6880
ResNet-50 ( <i>pool</i> )	0.6751	0.7047
ViT ( <i>pool</i> )	0.6661	0.7082
VGG-16 ( <i>layer stack</i> )	0.7513	0.7700
ResNet-50 ( <i>layer stack</i> )	0.7630	0.7828
VGG-16+ViT ( <i>pool+pool</i> )	0.7100	0.7364
ResNet-50+ViT ( <i>pool+pool</i> )	0.7253	0.7469
VGG-16+ViT ( <i>layer stack+pool</i> )	0.7650	0.7827
ResNet-50+ViT ( <i>layer stack+pool</i> )	0.7697	0.7897

indicates that ReLaX-VQA better captures the perception of quality in the vast video parameter space, indicating a wide adaptability and strong generalisation ability (see Table 5 the Appendix for the full results).

### 4.3 Ablation studies

In our ablation study, we explored the influence of different components on the performance of our proposed method. In the first part (see Table 3), we compare the spatio-temporal features: frame difference and optical flow, along with their performance after residual fragment (RF) sampling and merged fragment (MF). We found that RF sampling of frame difference and optical flow can notably improve performance, especially when using ViT to extract frame difference features, with SRCC and PLCC improving by about 11.92% and 11.96%, respectively. The combination of ResNet-50 and ViT enhances performance by about 7.83% (SRCC) and 7.41% (PLCC) compared to using ResNet-50 alone, and by about 3.71% (SRCC) and 3.32% (PLCC) compared to using ViT alone to extract features. This result emphasizes the effectiveness of multiple DNN integration strategies in dealing with complex video content and the importance of preserving inter-frame spatio-temporal variations for video quality assessment.

In the second part (Table 4), we compare the layer stack and pool features of different DNNs. The results show that the layer-stacking framework captures complex video features more effectively compared to the pooling framework. In particular, the combination of ResNet-50 and ViT, layer stack + pool features, achieves SRCC of 0.7697 and PLCC of 0.7897, which is noticeably better than using only pooled features. This demonstrates the benefits of the layer-stacking framework in capturing and exploiting deep network features. Here, since ViT is based on the self-attention mechanism, we do not use a layer-stacking framework for this.

## 5 Conclusion and future work

In this paper, we proposed ReLaX-VQA to address the challenge of NR-VQA for UGC videos. We used the residual difference and optical flow fragments between successive sampled frames to capture the spatio-temporal information. Additionally, we enhanced DNN features by stacking layers to capture local and global information affecting video quality. We trained and tested our model on four public UGC datasets. Our results showed that ReLaX-VQA outperforms existing NR-VQA methods and demonstrates consistently high performance across the different datasets, achieving an overall average SRCC value of 0.8658 and PLCC value of 0.8872. Our method verified the benefit of residual information in enhancing the perceptual capability of NR-VQA models. Future research will focus on efficiency through the use of network architectures such as Swin Transformer or Mamba for feature extraction, as well as on the improvement of regression (e.g., KAN).

## Acknowledgments

This work was funded by the UKRI MyWorld Strength in Places Programme (SIPF00006/1).

## References

- [1] Sandvine, “The global internet phenomena report.” <https://www.sandvine.com/blog/sandvines-2024-global-internet-phenomena-report-global-internet-usage-continues-to-grow>. [Online; accessed 16-May-2024].
- [2] B. Adsumilli, S. Inguva, Y. Wang, J. Huoponen, and R. Wolf, “Launching a YouTube dataset of user-generated content,” 2019.
- [3] Y. Wang, S. Inguva, and B. Adsumilli, “Youtube ugc dataset for video compression research,” in *2019 IEEE 21st International Workshop on Multimedia Signal Processing (MMSP)*, pp. 1–5, IEEE, 2019.
- [4] Z. Wang, A. C. Bovik, H. R. Sheikh, and E. P. Simoncelli, “Image quality assessment: from error visibility to structural similarity,” *IEEE transactions on image processing*, vol. 13, no. 4, pp. 600–612, 2004.
- [5] Z. Li, A. Aaron, I. Katsavounidis, A. Moorthy, and M. Manohara, “Toward a practical perceptual video quality metric,” *The Netflix Tech Blog*, vol. 6, no. 2, 2016.
- [6] L. Alzubaidi, J. Zhang, A. J. Humaidi, A. Al-Dujaili, Y. Duan, O. Al-Shamma, J. Santamaría, M. A. Fadhel, M. Al-Amidie, and L. Farhan, “Review of deep learning: concepts, cnn architectures, challenges, applications, future directions,” *Journal of big Data*, vol. 8, pp. 1–74, 2021.
- [7] W. Liu, Z. Duanmu, and Z. Wang, “End-to-end blind quality assessment of compressed videos using deep neural networks.,” in *ACM Multimedia*, pp. 546–554, 2018.
- [8] D. Li, T. Jiang, and M. Jiang, “Quality assessment of in-the-wild videos,” in *Proceedings of the 27th ACM International Conference on Multimedia*, pp. 2351–2359, 2019.
- [9] Z. Tu, X. Yu, Y. Wang, N. Birkbeck, B. Adsumilli, and A. C. Bovik, “Rapique: Rapid and accurate video quality prediction of user generated content,” *IEEE Open Journal of Signal Processing*, vol. 2, pp. 425–440, 2021.
- [10] Z. Ying, M. Mandal, D. Ghadiyaram, and A. Bovik, “Patch-vq: patching up the video quality problem,” in *Proceedings of the IEEE/CVF conference on computer vision and pattern recognition*, pp. 14019–14029, 2021.
- [11] W. Sun, X. Min, W. Lu, and G. Zhai, “A deep learning based no-reference quality assessment model for ugc videos,” in *Proceedings of the 30th ACM International Conference on Multimedia*, pp. 856–865, 2022.
- [12] H. Wu, C. Chen, L. Liao, J. Hou, W. Sun, Q. Yan, and W. Lin, “Discovqa: Temporal distortion-content transformers for video quality assessment,” *IEEE Transactions on Circuits and Systems for Video Technology*, 2023.
- [13] K. Zhao, K. Yuan, M. Sun, and X. Wen, “Zoom-vqa: Patches, frames and clips integration for video quality assessment,” in *Proceedings of the IEEE/CVF Conference on Computer Vision and Pattern Recognition*, pp. 1302–1310, 2023.
- [14] H. Wu, C. Chen, J. Hou, L. Liao, A. Wang, W. Sun, Q. Yan, and W. Lin, “Fast-vqa: Efficient end-to-end video quality assessment with fragment sampling,” in *European conference on computer vision*, pp. 538–554, Springer, 2022.
- [15] V. Sze, Y.-H. Chen, T.-J. Yang, and J. S. Emer, “Efficient processing of deep neural networks: A tutorial and survey,” *Proceedings of the IEEE*, vol. 105, no. 12, pp. 2295–2329, 2017.
- [16] J. You, “Long short-term convolutional transformer for no-reference video quality assessment,” in *Proceedings of the 29th ACM International Conference on Multimedia*, pp. 2112–2120, 2021.
- [17] P. C. Madhusudana, N. Birkbeck, Y. Wang, B. Adsumilli, and A. C. Bovik, “Conviqt: Contrastive video quality estimator,” *IEEE Transactions on Image Processing*, 2023.
- [18] ITU-T Rec. H.264, “Advanced video coding for generic audiovisual services,” 2005.
- [19] ITU-T Rec H.265, “High efficiency video coding,” 2015.
- [20] K. He, X. Zhang, S. Ren, and J. Sun, “Deep residual learning for image recognition,” in *Proceedings of the IEEE conference on computer vision and pattern recognition*, pp. 770–778, 2016.
- [21] A. Vaswani, N. Shazeer, N. Parmar, J. Uszkoreit, L. Jones, A. N. Gomez, Ł. Kaiser, and I. Polosukhin, “Attention is all you need,” *Advances in neural information processing systems*, vol. 30, 2017.
- [22] M. Nuutinen, T. Virtanen, M. Vaahteranoksa, T. Vuori, P. Oittinen, and J. Häkkinen, “CVD2014—A database for evaluating no-reference video quality assessment algorithms,” *IEEE Transactions on Image Processing*, vol. 25, no. 7, pp. 3073–3086, 2016.
- [23] V. Hosu, F. Hahn, M. Jenadeleh, H. Lin, H. Men, T. Szirányi, S. Li, and D. Saupe, “The konstanz natural video database (konvid-1k),” in *2017 Ninth international conference on quality of multimedia experience (QoMEX)*, pp. 1–6, IEEE, 2017.

- [24] Z. Sinno and A. C. Bovik, "Large-scale study of perceptual video quality," *IEEE Transactions on Image Processing*, vol. 28, no. 2, pp. 612–627, 2018.
- [25] S. Dodge and L. Karam, "Understanding how image quality affects deep neural networks," in *2016 eighth international conference on quality of multimedia experience (QoMEX)*, pp. 1–6, IEEE, 2016.
- [26] D. Ghadiyaram, J. Pan, A. C. Bovik, A. K. Moorthy, P. Panda, and K.-C. Yang, "In-capture mobile video distortions: A study of subjective behavior and objective algorithms," *IEEE Transactions on Circuits and Systems for Video Technology*, vol. 28, no. 9, pp. 2061–2077, 2017.
- [27] F. Götz-Hahn, V. Hosu, H. Lin, and D. Saupe, "No-reference video quality assessment using multi-level spatially pooled features," *arXiv preprint arXiv:1912.07966*, 2019.
- [28] A. Mittal, R. Soundararajan, and A. C. Bovik, "Making a "completely blind" image quality analyzer," *IEEE Signal processing letters*, vol. 20, no. 3, pp. 209–212, 2012.
- [29] A. K. Moorthy and A. C. Bovik, "Blind image quality assessment: From natural scene statistics to perceptual quality," *IEEE transactions on Image Processing*, vol. 20, no. 12, pp. 3350–3364, 2011.
- [30] A. Mittal, A. K. Moorthy, and A. C. Bovik, "Blind/referenceless image spatial quality evaluator," in *2011 conference record of the forty fifth asilomar conference on signals, systems and computers (ASILOMAR)*, pp. 723–727, IEEE, 2011.
- [31] M. A. Saad, A. C. Bovik, and C. Charrier, "Blind prediction of natural video quality," *IEEE Transactions on Image Processing*, vol. 23, no. 3, pp. 1352–1365, 2014.
- [32] J. Xu, P. Ye, Y. Liu, and D. Doermann, "No-reference video quality assessment via feature learning," in *2014 IEEE International Conference on Image Processing (ICIP)*, pp. 491–495, 2014.
- [33] J. Korhonen, "Two-level approach for no-reference consumer video quality assessment," *IEEE Transactions on Image Processing*, vol. 28, no. 12, pp. 5923–5938, 2019.
- [34] Z. Tu, Y. Wang, N. Birkbeck, B. Adsumilli, and A. C. Bovik, "Ugc-vqa: Benchmarking blind video quality assessment for user generated content," *IEEE Transactions on Image Processing*, vol. 30, pp. 4449–4464, 2021.
- [35] D. Li, T. Jiang, and M. Jiang, "Unified quality assessment of in-the-wild videos with mixed datasets training," *International Journal of Computer Vision*, vol. 129, no. 4, pp. 1238–1257, 2021.
- [36] Y. Liu, Y. Quan, G. Xiao, A. Li, and J. Wu, "Scaling and masking: A new paradigm of data sampling for image and video quality assessment," *arXiv preprint arXiv:2401.02614*, 2024.
- [37] J. Ke, T. Zhang, Y. Wang, P. Milanfar, and F. Yang, "Mret: Multi-resolution transformer for video quality assessment," *Frontiers in Signal Processing*, vol. 3, p. 1137006, 2023.
- [38] S. Lao, Y. Gong, S. Shi, S. Yang, T. Wu, J. Wang, W. Xia, and Y. Yang, "Attentions help cnns see better: Attention-based hybrid image quality assessment network," in *Proceedings of the IEEE/CVF conference on computer vision and pattern recognition*, pp. 1140–1149, 2022.
- [39] A.-X. Zhang, Y.-G. Wang, W. Tang, L. Li, and S. Kwong, "Hvs revisited: A comprehensive video quality assessment framework," *arXiv preprint arXiv:2210.04158*, 2022.
- [40] C. Feng, D. Danier, F. Zhang, and D. Bull, "Rankdvqa: Deep vqa based on ranking-inspired hybrid training," in *Proceedings of the IEEE/CVF Winter Conference on Applications of Computer Vision (WACV)*, pp. 1648–1658, January 2024.
- [41] B. Li, W. Zhang, M. Tian, G. Zhai, and X. Wang, "Blindly assess quality of in-the-wild videos via quality-aware pre-training and motion perception," *IEEE Transactions on Circuits and Systems for Video Technology*, vol. 32, no. 9, pp. 5944–5958, 2022.
- [42] Y. Wang, J. Ke, H. Talebi, J. G. Yim, N. Birkbeck, B. Adsumilli, P. Milanfar, and F. Yang, "Rich features for perceptual quality assessment of ugc videos," in *Proceedings of the IEEE/CVF Conference on Computer Vision and Pattern Recognition*, pp. 13435–13444, 2021.
- [43] G. Farneböck, "Two-frame motion estimation based on polynomial expansion," in *Image Analysis: 13th Scandinavian Conference, SCIA 2003 Halmstad, Sweden, June 29–July 2, 2003 Proceedings 13*, pp. 363–370, Springer, 2003.
- [44] X. Wang, A. Katsenou, and D. Bull, "Ugc quality assessment: exploring the impact of saliency in deep feature-based quality assessment," in *Applications of Digital Image Processing XLVI*, vol. 12674, pp. 351–365, SPIE, 2023.
- [45] D. Ramsook and A. Kokaram, "Learnt deep hyperparameter selection in adversarial training for compressed video enhancement with a perceptual critic," in *2023 IEEE International Conference on Image Processing (ICIP)*, pp. 2420–2424, 2023.
- [46] F. Rosenblatt, "The perceptron: a probabilistic model for information storage and organization in the brain.," *Psychological review*, vol. 65, no. 6, p. 386, 1958.

- [47] I. Loshchilov and F. Hutter, “Sgdr: Stochastic gradient descent with warm restarts,” *arXiv preprint arXiv:1608.03983*, 2016.
- [48] P. Izmailov, D. Podoprikin, T. Garipov, D. Vetrov, and A. G. Wilson, “Averaging weights leads to wider optima and better generalization,” *arXiv preprint arXiv:1803.05407*, 2018.
- [49] S. Wen and J. Wang, “A strong baseline for image and video quality assessment,” *arXiv preprint arXiv:2111.07104*, 2021.
- [50] K. Seshadrinathan, R. Soundararajan, A. C. Bovik, and L. K. Cormack, “Study of subjective and objective quality assessment of video,” *IEEE transactions on Image Processing*, vol. 19, no. 6, pp. 1427–1441, 2010.
- [51] A. Krizhevsky, I. Sutskever, and G. E. Hinton, “Imagenet classification with deep convolutional neural networks,” *Advances in neural information processing systems*, vol. 25, 2012.
- [52] A. Jadon, “Visualizing attention in vision transformer,” *Medium*, Jan 2023.
- [53] A. Paszke, S. Gross, F. Massa, A. Lerer, J. Bradbury, G. Chanan, T. Killeen, Z. Lin, N. Gimeshin, L. Antiga, *et al.*, “Pytorch: An imperative style, high-performance deep learning library,” *Advances in neural information processing systems*, vol. 32, 2019.

## A Appendix

### A.1 Framework: DNN layer stack module

We stacked the extracted features using different layers of the deep neural network, fusing these multi-layered features to capture the quality-aware features. Finally, a simple MLP quality regression module maps the quality-aware features to video quality scores. Here, since ViT is based on the self-attention mechanism, we do not use a layer-stacking framework for this, shown in Fig. 2

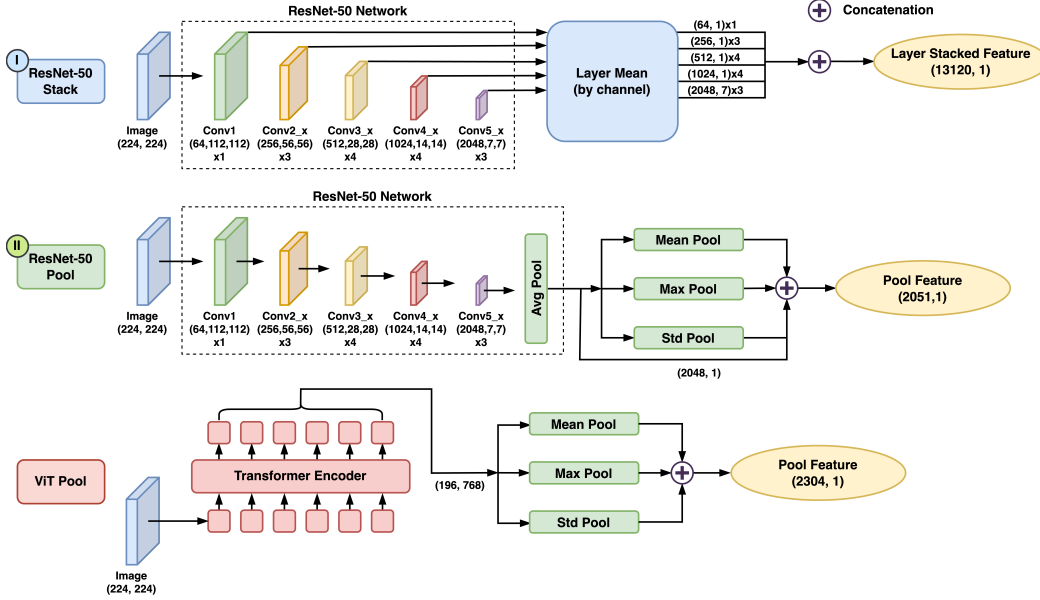


Figure 2: The bespoke architectures of ResNet-50 Stack (I) and ResNet-50 Pool (II).

### A.2 Spatio-temporal fragment sampling module

Here, we present the sampled frames and their corresponding ViT attention visualisations, along with the merged fragments (ours) and their ViT attention. These visualisations highlight the attention focus of the model. As shown in Fig. 3, the first video, *TelevisionClip\_1080P - 68c6.mkv*, is a clip showing a man wearing an Angry Birds print moving in a snowy environment. The second video *Sports\_2160P - 0455.mkv* shows changes in perspective during the motions, including significant jittering. The videos can be downloaded and viewed at <https://media.withoutube.com/>. Notice, that we get good results even when using our frozen ReLaX-VQA model without fine-tuning (ReLaX-VQA (w/o FT) to predict video quality scores.

### A.3 Nonlinear four-parameter logistic regression

In our experiments, PLCC and RMSE are calculated after a nonlinear four-parameter logistic regression[50], where  $\beta$  parameters were fitted using least squares.

$$f(x) = \beta_2 + \frac{\beta_1 - \beta_2}{1 + e^{-x + \frac{\beta_3}{|\beta_4|}}}, \quad (15)$$

### A.4 Performance comparison

We used the following datasets to train and evaluate our proposed model, CVD2014, KoNViD-1k, LIVE-VQC, YouTube-UGC and the largest dataset available, LSVQ. Based on the different strategies for training and testing we created three versions of our proposed method, ReLaX-VQA:

- i ReLaX-VQA: this version was separately trained and tested on each dataset;

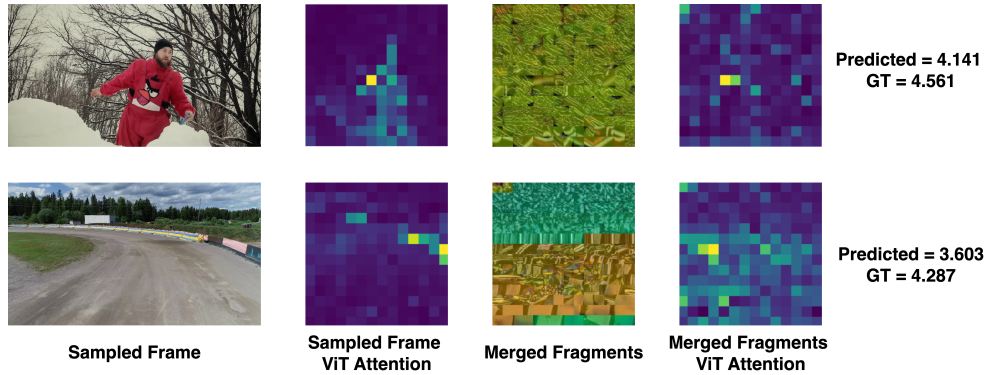


Figure 3: Illustration of examples sampled from the YouTube-UGC[3] dataset. **Top-row:** *TelevisionClip\_1080P – 68c6.mkv*. **Bottom-row:** *Sports\_2160P – 0455.mkv*. GT refers to ground truth quality scores. Shown here are the scores predicted using **ReLaX-VQA (w/o FT)**

- ii ReLaX-VQA (w/o FT): this version was trained on LSVQ dataset and the frozen model was used for testing on the other datasets;
- iii ReLaX-VQA (w/ FT): this version was trained on LSVQ dataset and the frozen model was fine-tuned on the other datasets to fit the new data features better.

We reported the SRCC, KRCC, PLCC, and RMSE metrics, along with the standard deviation (std) intervals, in Table 5. We need to note that for VSFA evaluation, we excluded the 110 2160p videos from the YouTube-UGC dataset because our GPU could not support them. It is worth noting that for these metrics, we tested our frozen models using the same divisional test set as for the other NR-VQAs (ReLaX-VQA (w/o FT) and ReLaX-VQA (w/ FT)). Therefore, we performed only one test and the standard deviation intervals were not included. We included more results and tests in the supplementary materials.

Table 5: Full performance comparison of the evaluated NR-VQA models on the four NR-VQA datasets. The red and blue entries indicate the best and second-best performance on each database for each performance metric, respectively.

Datasets		CVD2014[22]			
Models/Metrics	SRCC( $\pm$ STD)	KRCC( $\pm$ STD)	PLCC( $\pm$ STD)	RMSE( $\pm$ STD)	
BRISQUE[30]	0.5553 ( $\pm$ 0.0231)	0.3895 ( $\pm$ 0.0161)	0.5527 ( $\pm$ 0.0627)	18.4752 ( $\pm$ 1.0274)	
V-BLIINDS[31]	0.7306 ( $\pm$ 0.0511)	0.5393 ( $\pm$ 0.0473)	0.7853 ( $\pm$ 0.0414)	13.7267 ( $\pm$ 1.2130)	
TLVQM[33]	0.5399 ( $\pm$ 0.0352)	0.4006 ( $\pm$ 0.0298)	0.5785 ( $\pm$ 0.0498)	18.0832 ( $\pm$ 0.7052)	
VIDEVAL[34]	0.7663 ( $\pm$ 0.0214)	0.5634 ( $\pm$ 0.0221)	0.8062 ( $\pm$ 0.0216)	13.1151 ( $\pm$ 0.6579)	
RAPIQUE[9]	0.8530 ( $\pm$ 0.0301)	0.6836 ( $\pm$ 0.0357)	0.8766 ( $\pm$ 0.0326)	10.6670 ( $\pm$ 1.1939)	
VSFA†[8]	0.8825	0.7179	0.8784	9.8619	
<b>ReLaX-VQA (ours)</b>	0.8643 ( $\pm$ 0.0301)	0.6960 ( $\pm$ 0.0442)	0.8895 ( $\pm$ 0.0255)	9.8185 ( $\pm$ 1.0969)	
<b>ReLaX-VQA (w/o FT)</b>	0.7845	0.5930	0.8336	12.2445	
<b>ReLaX-VQA (w/ FT)</b>	0.8974	0.7299	0.9294	8.1812	

Datasets		KoNViD-1k[23]			
Models/Metrics	SRCC( $\pm$ STD)	KRCC( $\pm$ STD)	PLCC( $\pm$ STD)	RMSE( $\pm$ STD)	
BRISQUE[30]	0.6781 ( $\pm$ 0.0083)	0.4935 ( $\pm$ 0.0091)	0.6746 ( $\pm$ 0.0069)	0.4753 ( $\pm$ 0.0040)	
V-BLIINDS[31]	0.7258 ( $\pm$ 0.0115)	0.5322 ( $\pm$ 0.0109)	0.7155 ( $\pm$ 0.0107)	0.4498 ( $\pm$ 0.0071)	
TLVQM[33]	0.7616 ( $\pm$ 0.0067)	0.5635 ( $\pm$ 0.0067)	0.7463 ( $\pm$ 0.0065)	0.4285 ( $\pm$ 0.0047)	
VIDEVAL[34]	0.8073 ( $\pm$ 0.0174)	0.6036 ( $\pm$ 0.0165)	0.7923 ( $\pm$ 0.0169)	0.3928 ( $\pm$ 0.0133)	
RAPIQUE[9]	0.8219 ( $\pm$ 0.0057)	0.6264 ( $\pm$ 0.0074)	0.8191 ( $\pm$ 0.0079)	0.3693 ( $\pm$ 0.0070)	
VSFA†[8]	0.8067	0.6102	0.8182	0.4056	
<b>ReLaX-VQA (ours)</b>	0.8535 ( $\pm$ 0.0218)	0.6594 ( $\pm$ 0.0232)	0.8473 ( $\pm$ 0.0214)	0.3370 ( $\pm$ 0.0185)	
<b>ReLaX-VQA (w/o FT)</b>	0.8312	0.6418	0.8427	0.3466	
<b>ReLaX-VQA (w/ FT)</b>	0.8720	0.6881	0.8668	0.3211	

Datasets		LIVE-VQC[24]			
Models/Metrics	SRCC( $\pm$ STD)	KRCC( $\pm$ STD)	PLCC( $\pm$ STD)	RMSE( $\pm$ STD)	
BRISQUE[30]	0.6096 ( $\pm$ 0.0133)	0.4420 ( $\pm$ 0.0127)	0.6652 ( $\pm$ 0.0176)	12.7480 ( $\pm$ 0.2697)	
V-BLIINDS[31]	0.6925 ( $\pm$ 0.0103)	0.5046 ( $\pm$ 0.0111)	0.6872 ( $\pm$ 0.0124)	12.4031 ( $\pm$ 0.1948)	
TLVQM[33]	0.8133 ( $\pm$ 0.0104)	0.6231 ( $\pm$ 0.0105)	0.7912 ( $\pm$ 0.0148)	10.4409 ( $\pm$ 0.3123)	
VIDEVAL[34]	0.7725 ( $\pm$ 0.0093)	0.5874 ( $\pm$ 0.0080)	0.7752 ( $\pm$ 0.0211)	10.7846 ( $\pm$ 0.4082)	
RAPIQUE[9]	0.7328 ( $\pm$ 0.0130)	0.5418 ( $\pm$ 0.0134)	0.7520 ( $\pm$ 0.0119)	11.2538 ( $\pm$ 0.2285)	
VSFA†[8]	0.5898	0.4120	0.5894	15.3245	
<b>ReLaX-VQA (ours)</b>	0.7655 ( $\pm$ 0.0378)	0.5785 ( $\pm$ 0.0365)	0.8079 ( $\pm$ 0.0352)	9.8596 ( $\pm$ 0.9099)	
<b>ReLaX-VQA (w/o FT)</b>	0.7664	0.5812	0.8242	9.8201	
<b>ReLaX-VQA (w/ FT)</b>	0.8468	0.6649	0.8876	7.9869	

Datasets		YouTube-UGC[3]			
Models/Metrics	SRCC( $\pm$ STD)	KRCC( $\pm$ STD)	PLCC( $\pm$ STD)	RMSE( $\pm$ STD)	
BRISQUE[30]	0.3517 ( $\pm$ 0.0165)	0.2416 ( $\pm$ 0.0119)	0.3768 ( $\pm$ 0.0200)	0.6349 ( $\pm$ 0.0056)	
V-BLIINDS[31]	0.4783 ( $\pm$ 0.0188)	0.3396 ( $\pm$ 0.0143)	0.4967 ( $\pm$ 0.0228)	0.5949 ( $\pm$ 0.0094)	
TLVQM[33]	0.6802 ( $\pm$ 0.0183)	0.4892 ( $\pm$ 0.0168)	0.6876 ( $\pm$ 0.0207)	0.4977 ( $\pm$ 0.0132)	
VIDEVAL[34]	0.7814 ( $\pm$ 0.0049)	0.5906 ( $\pm$ 0.0052)	0.7929 ( $\pm$ 0.0038)	0.4177 ( $\pm$ 0.0033)	
RAPIQUE[9]	0.7994 ( $\pm$ 0.0064)	0.5989 ( $\pm$ 0.0054)	0.8300 ( $\pm$ 0.0070)	0.3823 ( $\pm$ 0.0068)	
VSFA†[8]	0.7857	0.5814	0.7808	0.4321	
<b>ReLaX-VQA (ours)</b>	0.8014 ( $\pm$ 0.0196)	0.6167 ( $\pm$ 0.0193)	0.8204 ( $\pm$ 0.0186)	0.3801 ( $\pm$ 0.0177)	
<b>ReLaX-VQA (w/o FT)</b>	0.8104	0.6131	0.8354	0.3768	
<b>ReLaX-VQA (w/ FT)</b>	0.8469	0.6623	0.8652	0.3437	